
Robust and highly adaptable brain–computer interface with convolutional net architecture based on a generative model of neuromagnetic measurements

Ivan Zubarev ^{*†}Rasmus Zetter [†]Hanna-Leena Halme [†]Lauri Parkkonen ^{†‡}

Abstract

Deep Neural Networks have been applied very successfully in image recognition and natural language processing. Recently these powerful methods have received attention also in the brain–computer-interface (BCI) community. Here, we introduce a convolutional neural network (CNN) architecture optimized for classification of brain states from non-invasive magnetoencephalographic (MEG) measurements. The model structure is motivated by a state-of-the-art generative model of the MEG signal and is thus readily interpretable in neurophysiological terms. We demonstrate that the proposed model is highly accurate in decoding event-related responses as well as modulations of oscillatory brain activity, and is robust with respect to inter-individual differences. Importantly, the model generalizes well across users: when trained on data pooled from previous users, it can successfully perform on new users. Thus, the time-consuming BCI calibration can be omitted. Moreover, the model can be incrementally updated, resulting in +8.9% average accuracy improvement in offline experiments and +17.0% in a real-time BCI. We argue that this model can be used in practical BCIs and basic neuroscience research.

1 Introduction

Deep Neural Networks (DNNs) are powerful tools which outperform traditional classification methods in many domains. However, their practical application to BCIs is limited due to the fact that the acquisition of sufficiently large amounts of neuroimaging data is expensive and time-consuming.

One way to overcome this limitation is to design a DNN that can be trained on other subjects and applied to new users. To generalize across subjects, such models need to be robust with respect to measurement noise and distortions due to inter- and intra-subject variability. Thus, the high complexity of DNNs should be effectively constrained by introducing reasonable assumptions about the nature of the signal of interest.

In this work, we propose a convolutional neural network (CNN) whose architecture is inspired by a generative model of non-invasive electromagnetic measurements (Daunizeau and Friston, 2007). Specifically, we encode our prior knowledge of the linear properties of spatial mixing and non-linear temporal dynamics into the network architecture.

^{*}Corresponding author ivan.zubarev@aalto.fi

[†]Department of Neuroscience and Biomedical Engineering, Aalto University, Espoo, Finland

[‡]Aalto Neuroimaging, Aalto University, Espoo, Finland

We apply this neural network to classify evoked responses to sensory stimuli (5 and 8 classes; Experiment 1) and oscillatory responses induced by hand motor imagery and rest (3 classes; Experiment 2). Finally, we test the method in a real-time BCI experiment (2 classes; Experiment 3). All experiments show higher classification performance and interpretability compared to the benchmark methods.

Importantly, we demonstrate that the model transfers successfully when applied to the data from new subjects. By using the proposed model, we can achieve state-of-the-art BCI accuracy without a separate calibration session by initializing the BCI using pooled data of other subjects performing a similar task. Moreover, we use the iterative nature of DNN training to achieve even higher real-time accuracies by updating this model incrementally as new observations arrive in both simulated (Experiments 1 and 2) and true (Experiment 3) real-time MEG-based BCIs. Furthermore, this approach – mimicking the traditional analysis of neuroimaging data – allows a domain expert to interpret the network parameters with regard to the underlying brain activity.

Contributions summary We introduce two compact CNN models optimized for across-subject classification of neuromagnetic measurements. We also propose to use stochastic updates in a real-time BCI measurement to improve the model performance. Finally, for the first time, we demonstrate a real-time application of a CNN in a BCI.

This paper is organized as follows. Section 2 briefly introduces MEG and the theoretical assumptions motivating the proposed network design. In Sections 3 and 4, we introduce the new CNN architectures and benchmark models used in our study. Section 5 describes the experiments and datasets and finally Section 6 comprises the results and a discussion of the key observations and related work.

2 Magnetoencephalography

Magnetoencephalography (MEG) is a non-invasive, time-resolved technique for measuring electric brain activity through the magnetic field it generates (Hämäläinen et al., 1993). The MEG signal is complementary to that of electroencephalography (EEG), in which the potential distribution caused by electric brain activity is measured using electrodes placed on the scalp. MEG is considered to have higher spatial resolution than EEG, as the EEG signal is distorted by the heterogeneous conductivity profile of head tissues to a much larger extent than the MEG signal (see e.g. Baillet, 2017).

MEG signals include 1) stereotyped evoked responses (event-related fields; ERF) that are phase-locked to specific sensory, cognitive or motor events, and 2) induced modulations of ongoing oscillatory brain activity that is not phase-locked to external events. MEG measurements are typically contaminated by noise and interference originating from external sources as well as by ongoing unrelated brain activity. Unaveraged ERFs typically have a signal-to-noise ratio (SNR) ~ 1 .

A MEG measurement can be represented by an $n \times t$ data matrix \mathbf{X} containing measurements from n sensors (magnetometers or gradiometers; typ. 200–300) at t time points sampled at a high temporal frequency (typ. ~ 1000 Hz). These data have a complex spatiotemporal structure because an activation of a single neural source is picked up by several sensors at different spatial locations and these signals exhibit temporal correlations (e.g. they could have a specific frequency fingerprint). Thus, simultaneously active neural sources result in a high degree of linear spatial mixing and non-linear temporal dependencies in the measured data. Fortunately, spatial and temporal oversampling as well as acquiring a large number of responses to the same stimulus or task enables extracting this structure from the data. Therefore, an effective approach towards decoding brain states should take into account these properties of the signal.

2.1 Generative latent state-space model of MEG data

The proposed network architecture is broadly based on an extension of a model describing the generation of MEG signal (Daunizeau and Friston, 2007). The model is motivated by the assumption that a single event-related MEG observation $\mathbf{X} \in \mathbb{R}^{n \times t}$ is generated by a mixture of k latent sources s such that at each time point t

$$\mathbf{X}_t = \mathbf{f}(\mathbf{C}\mathbf{S}_t) + \epsilon \quad (1)$$

where \mathbf{C} is $n \times k$ matrix describing the mixing of k underlying latent sources, and ϵ is additive observation noise. \mathbf{S} is a $k \times t$ matrix describing the time courses of the k latent sources with additive innovation noise ω . These sources evolve in time in a structured way and may or may not be

statistically dependent. The number of such latent sources is small relative to the number of MEG channels (i.e. $k \ll n$). Importantly, we do not restrict the definition of a latent source to neural activity as some of these sources may correspond to e.g. ocular or muscular artifacts in the data. In the simplest case, mapping from \mathbf{S} to \mathbf{X} is linear, and non-linearities in temporal dynamics of \mathbf{S} can be locally approximated by an autoregressive model \mathbf{A} of order L . Thus,

$$\mathbf{S}_t = \mathbf{g}\left(\sum_{l=1}^L \mathbf{A}_l \mathbf{S}_{t-l}\right) + \omega. \quad (2)$$

In the simplest linear case, both link functions $\mathbf{f}(\cdot)$ and $\mathbf{g}(\cdot)$ can be identity functions. Given the fast temporal sampling of MEG, such local linearity in the temporal domain is a reasonable assumption.

3 Network architecture

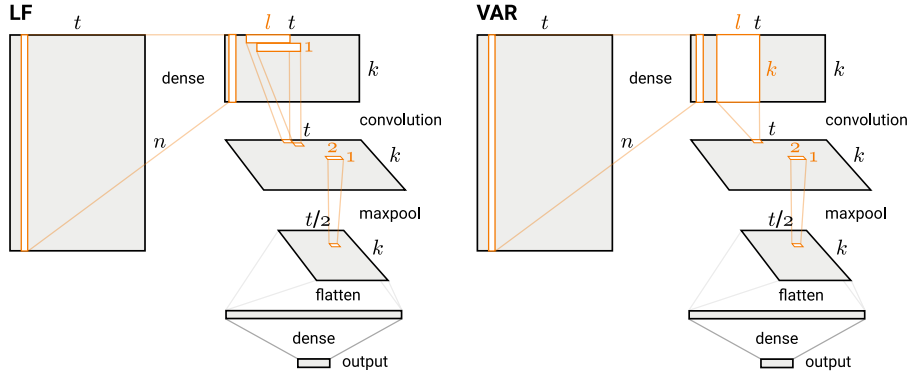


Figure 1: Network architecture of both the LF- and VAR-CNN variants.

Input layer: Linear spatial de-mixing The input layer is a fully-connected layer applying linear dimensionality reduction across the spatial domain. This layer trains a set of spatial filters that project the channel data onto a k -dimensional subspace. Similar linear projections are typically used to project out ocular and cardiac artifacts from the MEG data. However, our approach does not have as explicit modeling assumptions as in e.g. principal component analysis (PCA) or independent component analysis (ICA). Instead, we define the projection basis in a data-driven manner by backpropagation. This layer has several potential functions: (1) it obtains a lower-dimensional and spatially-decorrelated representation of the signal time courses, (2) it learns and projects out irrelevant activity such as physiological artifacts, (3) it provides an interpretable linear mapping from model weights back to spatial locations of the most informative channels in the original signal space. These weights, multiplied by the data covariance matrix, yield spatial activation patterns (Haufe et al., 2014), or topographic maps, corresponding to neural sources active in each condition. These spatial patterns can then be assessed by domain experts.

Temporal convolution layer We used two variants of this layer. The simpler one (LF-CNN) applies separate 1-dimensional convolution filters of the l -th order to the time courses of the k spatial components produced by the input layer. The model assumes that these time courses do not interact and that they have unique spectral fingerprints. This layer variant can be viewed as applying linear finite-impulse-response filters (hence LF) that specifically capture the fingerprint of each spatial component.

The more complex variant allows estimating the interactions between the spatial components and can be viewed as a Vector Autoregressive Model (VAR-CNN) of the component time courses. This structure is implemented by applying k spatiotemporal convolution kernels of shape $l \times k$ and results in a larger set of trainable parameters ($l \times k \times k$) in this layer. Thus, each spatial pattern from the input layer has a corresponding impulse-response function learned by the temporal convolution layer. These functions select the frequency bands specific for each component.

For both variants of this layer, the convolution is followed by a non-linearity using Rectified linear units (*ReLU*) and a max-pooling layer with a pooling factor of 2 and a stride of 2 applied to the time dimension.

Output layer The mapping from the temporal convolution layer to the output is provided by a single fully-connected layer with a soft-max non-linearity.

3.1 Model training

Initialization, cost function, performance metrics and optimization The initial values of the weight matrices were drawn from a truncated zero-mean normal distribution with a standard deviation (SD) of 0.1. Bias variables were initialized to a constant value of 0.1. We used the Adam optimization algorithm with a batch size of 100 and learning rate of $3.0 \cdot 10^{-4}$ to optimize multinomial cross-entropy between model predictions and true labels. Higher learning rates were also used but they did not improve performance. We used an early-stopping strategy to prevent over-fitting; for each 1000 iterations we computed the validation cost (multinomial cross entropy) and stopped the iterations immediately if the cost function value was increasing or decreasing by less than $1.0 \cdot 10^{-5}$. The early-stopping criteria were typically met within 20 000 iterations resulting in maximum training time of 32 minutes using a normal workstation CPU only.

Regularization We examined several regularization approaches including drop-out, l_1 and l_2 penalties on the model weights, as well as the pairwise combinations of drop-out with weight penalties. A combination of drop-out regularization applied to the output layer and l_1 penalty applied to all weight variables resulted in the highest model performance and was used with all datasets.

Across-subject performance evaluation Since the main focus of our study was on developing a model that generalizes across subjects, we used a leave-one-subject-out method to evaluate model performance. For a dataset of k subjects, the training (90% of all trials) and validation (10% of all trials) sets comprised randomly selected pooled data from $k - 1$ subjects. The model was then applied to the data of the held-out subject and two scores were computed. As all our datasets comprised an equal number of trials for each category, we used classification accuracy as the performance metric. *Initial test accuracy* was defined as the proportion of correct predictions on the held-out subject. *Pseudo-real-time accuracy* was defined as the mean prediction accuracy in a simulated real-time design where the model predicted new observations in batches of 20 trials and was updated after each prediction. For the true real-time BCI experiment (Experiment 3), the actual BCI accuracy (with and without model updates) is reported.

3.2 Model implementation

The neural network was implemented using the Tensorflow library (Abadi et al., 2016). Model development and hyperparameter tuning were performed on the data of a single randomly-picked subject from Dataset 1 and then applied to across-subject classification and other experiments as is. Table 1 summarizes the tunable hyperparameters used for different models.

Table 1: Model design options and final implementation

Parameter	Options	Final implementation
Number of latent sources	16, 32, 64	32
Temporal filter length	3, 5, 7, 9, 11	7
Learning rate	$1 \cdot 10^{-3}$, $3 \cdot 10^{-4}$, $1 \cdot 10^{-4}$	$3 \cdot 10^{-4}$
l_1 -penalty	$1 \cdot 10^{-3}$, $3 \cdot 10^{-4}$, $1 \cdot 10^{-4}$	$3 \cdot 10^{-4}$
Pooling	<i>max</i>	<i>max</i>
Pooling factor	2, 3, 5	2
Drop-out coefficient	0.25, 0.5, 0.75, 0.9	0.5
Input layer link function	<i>identity</i> , <i>ReLU</i> , <i>ELU</i> , <i>tanh</i>	<i>identity</i>
Hidden layer link function	<i>identity</i> , <i>ReLU</i> , <i>ELU</i> , <i>tanh</i>	<i>ReLU</i>
Output nonlinearity	<i>sigmoid</i> , <i>softmax</i>	<i>softmax</i>
Number of dense hidden layers	1, 2	1

3.3 Feature scaling

We used the same scaling approach for all three experiments. Each segment of MEG data was scaled independently by subtracting the mean and dividing by the standard deviation of the MEG signal immediately preceding the presentation of the stimulus (the $-300 \dots 0$ -ms interval with the zero time corresponding to the stimulus onset). This scaling approach was based on the fact that the evoked responses and modulations of oscillatory activity occur after the presentation of the stimulus, so the pre-stimulus interval can be used for estimating the noise level. Thus, our scaling recipe is a compromise between the standard baseline-correction method used in MEG applied to each channel independently, and the standard machine-learning practice of normalization across the whole observation.

4 Benchmark classifiers

4.1 RBF-SVM

We used a Support Vector Machine (SVM) classifier with a radial-basis-function (RBF) kernel, as implemented in scikit-learn, as a benchmark classifier (Pedregosa et al., 2011). RBF-SVMs (Vapnik, 2000) are widely used in classification of MEG data (e.g. Gramfort et al., 2013; Westner et al., 2018). The SVM inverse regularization parameter C and kernel lengthscale parameter γ were set by performing a search over a 2-d grid of 5 logarithmically spaced values from 10^3 to 10^5 for C and from 10^{-2} to 10^{-7} for γ . The classifier that resulted in highest validation set accuracy was evaluated on the test set.

4.2 CNNs developed for EEG classification

We used two CNN models developed for classification of EEG data. Shallow FBCSP-CNN (Schirrneister et al., 2017) is a model inspired by Filter-Bank Common Spatial Pattern (FBCSP), a state-of-the-art method for extracting band-power features in EEG/MEG. Its architecture comprises a 1-d temporal-convolution input layer (40 filters) followed by a spatial-filter layer (40 filters) and mean pooling. The outputs of the pooling layer are then combined linearly to produce label predictions by applying the soft-max function. We used the Shallow FBCSP-CNN implementation provided in the Braindecode library with default parameters, only modifying temporal filters and pooling factors to match the sampling rate of our data (125 Hz).

EEGnet (Lawhern et al., 2016) is a compact model designed specifically to optimize across-subject generalization. The model uses a combination of 1-d depth-wise and separable convolution layers (a total of 4 layers) and has been shown to generalize well across subjects in a large number of datasets. We implemented EEGNet-8 in Tensorflow following the description provided in Lawhern et al. (2016) and tested it in a simulated real-time set-up, similarly to VAR-CNN and LF-CNN.

5 Datasets

This section describes the datasets and preprocessing procedures applied to the MEG data in each of our experiments. All MEG recordings included in this work were acquired using an Elekta Neuromag Vectorview (Elekta Oy, Helsinki, Finland) MEG system, which includes 306 sensors at 102 positions around the head; two orthogonal planar gradiometers and a magnetometer at each position. Only data from the planar gradiometers (204 channels) were used in this work. The MEG dataset of Experiment 1 was preprocessed using a state-of-the-art off-line pipeline that is not applicable in a real-time BCI setting. Preprocessing the datasets from Experiments 2 and 3 was performed exclusively using methods available for real-time processing. The rationale for different preprocessing approaches was to progress from an optimal MEG pipeline (Experiment 1) to a reduced one, comprising only those methods that are available in a real-time setting (Experiment 2), and finally to demonstrate a real BCI experiment (Experiment 3).

5.1 Experiment 1: Event-related fields due to sensory stimuli

Dataset 1 comprised single-trial event-related field (ERF) responses in 7 healthy human subjects to 5 types of sensory stimuli; Gabor patches presented in the right or left visual hemifield (Classes 1 and

2), auditory tones presented to the left or right ear (pooled in to Class 3), and transient transcutaneous electrical stimulation of the median nerve at the left or right wrist (Classes 4 and 5). We also analyzed an extended 8-class version of this dataset including bilateral visual and somatosensory stimuli as well as separate classes for the left and right auditory stimuli (for the results, see Supplementary Table 2). Both dataset versions comprised 500-ms segments of MEG measurements sampled at 1000 Hz (500 samples measured by 204 MEG channels) starting at the onset of each stimulus. Total trial counts per subject were 1622 ± 322 (mean \pm SD).

External magnetic interference was suppressed and head movements compensated for using the temporally-extended signal-space separation (tSSS) method implemented in the MaxFilter software (version 2.2; Elekta Oy, Helsinki, Finland) (Taulu and Simola, 2006). Thereafter, cardiac and ocular artifacts were projected out using the FastICA algorithm as implemented in the MNE-Python software (Gramfort et al. 2013). The data were band-pass filtered to 1–45 Hz and downsampled to 125 Hz to minimize the number of features.

5.2 Experiment 2: Event-related perturbations of oscillatory activity in 3-class motor imagery task

Dataset 2 comprised MEG measurements of 17 healthy human subjects who performed a motor-imagery task (for details see Halme and Parkkonen (2016)), in which they imagined moving either their left or right hand (without any actual movement) when a visual cue was presented. The data comprised 1500-ms segments of MEG measurements sampled at 1000 Hz (1500 samples measured by 204 MEG channels) starting at the onset of the visual cue. Based on the measured MEG signal, we decoded whether the subject imagined moving his/her left or right hand, or no hand at all (rest condition). Total trial counts per subject were 82 ± 5 (mean \pm SD).

The data were band-pass filtered to 1–45 Hz and resampled to 125 Hz. No external magnetic interference suppression or artifact suppression was performed.

5.3 Experiment 3: Real-time motor-imagery BCI

In Experiment 3, we applied the same experimental paradigm as in Experiment 2, but with true real-time decoding and updating of the model. For this experiment, a network trained using data from 17 subjects (Experiment 2) was integrated into a real-time motor-imagery BCI in which we performed 2-class classification (left vs. right hand motor imagery). Two subjects performed a task where they had to imagine moving the left or right hand following the presentation of a visual cue (an arrow pointing to the left or to the right). None of the subjects had used motor-imagery based BCIs before or were involved in the collection of the MEG data used to train the model. The experiment comprised three sessions, and the cues in each session were presented in three different pre-defined random sequences (50 trials per session) so that the true labels were available for real-time accuracy estimation and incremental model optimization. The model parameters were updated following each successful trial by performing a single backpropagation step using the MEG data from this trial and the associated label. Data preprocessing was identical to that of Experiment 2.

6 Results

6.1 Experiment 1

In a 5-class classification of sensory ERFs, VAR-CNN outperformed other models in terms of accuracy on a pooled validation set ($95.2\% \pm 0.5$) but did not perform significantly better than RBF-SVM and LF-CNN on held-out subjects (85.0% vs. 82.3% , and 81.5% , respectively). In simulated real-time experiments, EEGNet-8, LF-CNN and VAR-CNN significantly improved their performance ($+13.1\%$, $+11.0\%$, and $+8.5\%$, respectively) compared to the initial test accuracies. These results are summarized in Table 2. Figure 2a shows the activation patterns and corresponding frequency responses extracted from the LF-CNN model trained on the data from Experiment 1. Each of these patterns resembles the topographic maps obtained via standard ERF analysis (e.g. the activation map on the left corresponds to sources in auditory cortex while the right one corresponds to sources in visual cortex).

Table 2: Across-subject performance in a 5-class sensory stimulation task. Grand-average accuracy scores (mean \pm SD) defined by leave-one-subject-out cross-validation.

Model	Validation (%)	Initial test (%)	Pseudo-real-time (%)	Train time (s)
LF-CNN	94.7 \pm 0.7	82.3 \pm 8.2	93.3 \pm 3.4	218 \pm 12
VAR-CNN	95.2 \pm 0.5	85.0 \pm 8.0	93.5 \pm 3.1	411 \pm 26
RBF-SVM	93.5 \pm 0.7	81.5 \pm 9.2	n.a.	426 \pm 25
EEGNet-8	85.1 \pm 1.1	70.4 \pm 10.4	83.5 \pm 5.5	3680 \pm 759
ShallowFBCSP-CNN	90.0 \pm 1.2	19.7 \pm 4.7	n.a.	14661 \pm 3270

6.2 Experiment 2

With the 3-class motor-imagery dataset, VAR-CNN resulted in slightly higher classification accuracies when applied to both pooled validation set (85.1% \pm 7.4) and to held-out subjects (75.6% \pm 7.3) compared to other models. Similarly to Experiment 1, both EEGNet-8, LF-CNN and VAR-CNN were able to significantly improve their performance in a simulated real-time test using incremental updates (+7.0%, +7.1%, and +6.8%, respectively) compared to the initial test accuracies.

Table 3: Across-subject performance in a 3-class motor imagery task. Grand-average accuracy scores (mean \pm SD) defined by leave-one-subject-out cross-validation.

Model	Validation (%)	Initial test (%)	Pseudo-real-time (%)	Train time (s)
LF-CNN	82.6 \pm 1.9	71.6 \pm 7.4	78.7 \pm 6.3	747 \pm 154
VAR-CNN	85.1 \pm 7.4	75.6 \pm 7.3	82.4 \pm 6.7	1493 \pm 259
RBF-SVM	79.2 \pm 1.6	72.1 \pm 7.5	n.a.	201 \pm 4
EEGNet-8	78.5 \pm 0.2	71.3 \pm 8.2	78.3 \pm 7.2	898 \pm 231
ShallowFBCSP-CNN	70.2 \pm 4.1	60.2 \pm 10.3	n.a.	240 \pm 34 ^a

Figure 2b shows two characteristic spatial activation maps of the LF-CNN model, which correspond to the motor cortices of either hemisphere.

6.3 Experiment 3: Real-time motor imagery BCI

Results of the real-time application of VAR-CNN are summarized in Table 4. Comparing the accuracies achieved by VAR-CNN with and without stochastic updates clearly shows the significant increase in performance. We note that since the subject had no prior experience with motor-imagery BCIs, the improvement in performance after Session 1 may be partly attributed to their improved motor-imagery skills.

Table 4: VAR-CNN classification accuracy in a real-time motor-imagery BCI experiment.

Subject	Run 1, no updates (%)	Run 2, online updates (%)	Run 3, online updates (%)
s01	80.0	88.0	92.0
s02	62.0	90.0	82.0

7 Discussion and related work

Related work Several studies report applying Deep Neural Networks (DNNs) to single-trial classification of non-invasive neurophysiological measurements, typically using multichannel EEG data. Most successful models make use of the spatiotemporal structure of EEG (Bashivan et al., 2015; Hajinoroozi et al., 2016; Lawhern et al., 2016; Schirrmeyer et al., 2017). Bashivan et al. (2015) exploit the spatiotemporal and spectral structure of EEG by transforming the signals into a sequence of multidimensional spatio-spectral images using time–frequency and polar transforms to achieve

^aRun on a computing cluster GPU node due to excessive training time and memory demand.

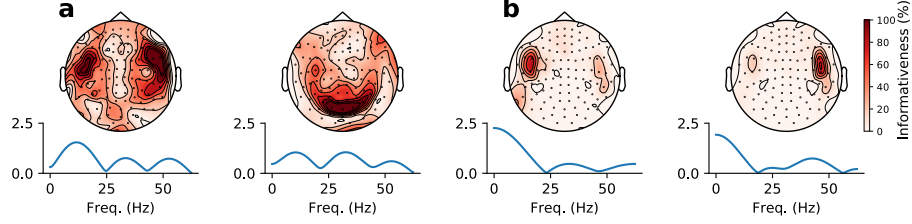


Figure 2: Two characteristic spatial activation maps and the corresponding filter responses extracted from LF-CNN input and convolution layers of Dataset 1 (a) and 2 (b). The topographic visualizations (upper row) correspond to channel locations (marked with dots) in relation to the head of the subject.

significant performance improvement in classifying cognitive load. By contrast, we use a simpler linear decomposition in the spatial domain. Similarly, Hajinoroozi et al. (2016) proposed spatial ICA as a preprocessing step followed by applying temporal 1-d convolution filters proven to be better suited for EEG data in several studies (Schirrneister et al., 2017; Shamwell et al., 2016). However, that did not result in a significant improvement in model performance compared to using EEG channel data as the input. We argue that – when performed separately from the classification – ICA decomposition may not be optimal due to the independence assumption which may not hold for real EEG and MEG signals. In our design, we relaxed the ICA assumption by optimizing spatial filters in conjunction with frequency filters in the temporal convolution layer. Such design allows us to obtain supervised decompositions related to a combination of Linear Discriminant Analysis (McLachlan, 1992), and Spatio-Spectral Decomposition (Nikulin et al., 2011) used in EEG-MEG analysis.

Lawhern et al. (2016) introduced the EEGNet model as a compact, interpretable CNN architecture that can be successfully applied to different EEG-based BCI paradigms (including both evoked and induced oscillatory responses). EEGNet has also been shown to generalize well when applied to held-out subjects. One particular advantage of EEGNet is the small number of trainable parameters allowing the model to be trained on the very limited training data typically available in BCI applications. We follow a similar approach, focusing on across-subject generalization and real-time applications.

Similarly to other models (e.g. Schirrneister et al., 2017), Lawhern et al. (2016) apply 1-d temporal convolutions to the raw EEG channel data. By contrast, we apply spatial decomposition first, followed by a temporal depth-wise (LF-CNN) or (spatio-temporal) (fully-connected) convolution (VAR-CNN). The motivation for this is three-fold: first, it allows effective spatial decorrelation and dimensionality reduction; second, when nested into the CNN architecture, it allows the network to learn and project out physiological artifacts similarly to other linear projection methods; finally, it can contribute to improved generalization across subjects by increasing model robustness to inter-individual differences. The latter argument is particularly important for MEG, since its spatial resolution is considerably higher than that of EEG, and even minor differences in source location or orientation may lead to different channels being the most sensitive to the brain activity of interest, which is also the likely reason why the CNN models optimized for EEG decoding did not perform optimally in our study.

To our knowledge, Halme and Parkkonen (2016) is the only study that provides a comprehensive comparison of the performance of domain-specific feature extraction and machine-learning techniques (not based on neural networks) with regard to applications for real-time MEG motor imagery BCIs. This study may serve as a point of reference to compare the performance of our model to other methods in MEG.

Conclusions We have introduced a Convolutional Neural Network model optimized for real-time BCI applications based on MEG. We show that this model can successfully perform when classifying multi-class ERFs and modulations of oscillatory activity in off-line experiments as well as in a real-time BCI experiment. Incorporating prior assumptions about the processes generating MEG observations into the architecture of our model allowed us to effectively reduce the model complexity while preserving high accuracy and interpretability. Importantly, this resulted in a model that is robust to inter-individual differences in MEG signal that – combined with the suggested incremental

real-time updates – can allow avoiding the time-consuming calibration sessions in MEG-based brain–computer interfaces once a sufficient amount of training data from other subjects is available.

References

- M. Abadi, P. Barham, J. Chen, Z. Chen, A. Davis, J. Dean, M. Devin, S. Ghemawat, G. Irving, M. Isard, et al. Tensorflow: A system for large-scale machine learning. In *OSDI*, volume 16, pages 265–283, 2016.
- S. Baillet. Magnetoencephalography for brain electrophysiology and imaging. *Nature Neuroscience*, 20(3):327–339, 2017. ISSN 1097-6256. doi: 10.1038/nn.4504.
- P. Bashivan, I. Rish, M. Yeasin, and N. Codella. Learning Representations from EEG with Deep Recurrent-Convolutional Neural Networks. 2015. ISSN 03610926. doi: 10.1080/03610928808829796.
- J. Daunizeau and K. J. Friston. A mesostate-space model for EEG and MEG. *NeuroImage*, 38(1): 67–81, 2007. ISSN 10538119. doi: 10.1016/j.neuroimage.2007.06.034.
- A. Gramfort, M. Luessi, E. Larson, D. A. Engemann, D. Strohmeier, C. Brodbeck, R. Goj, M. Jas, T. Brooks, L. Parkkonen, and M. Hämäläinen. MEG and EEG data analysis with MNE-Python. *Frontiers in neuroscience*, 7:267, 12 2013. ISSN 1662-4548. doi: 10.3389/fnins.2013.00267.
- M. Hajinorozi, Z. Mao, T.-P. Jung, C.-T. Lin, and Y. Huang. EEG-based prediction of driver’s cognitive performance by deep convolutional neural network. *Signal Processing: Image Communication*, 47:549–555, 2016.
- H.-L. Halme and L. Parkkonen. Comparing Features for Classification of MEG Responses to Motor Imagery. *PloS one*, 11(12):e0168766, 2016.
- M. S. Hämäläinen, R. Hari, R. J. Ilmoniemi, J. Knuutila, and O. V. Lounasmaa. Magnetoencephalography—theory, instrumentation, and applications to noninvasive studies of the working human brain. *Reviews of Modern Physics*, 65(2):413–505, apr 1993. ISSN 0034-6861. doi: 10.1103/RevModPhys.65.413.
- S. Haufe, F. Meinecke, K. Görgen, S. Dähne, J.-D. Haynes, B. Blankertz, and F. Bießmann. On the interpretation of weight vectors of linear models in multivariate neuroimaging. *NeuroImage*, 87: 96–110, 2014. ISSN 10959572. doi: 10.1016/j.neuroimage.2013.10.067.
- V. J. Lawhern, A. J. Solon, N. R. Waytowich, S. M. Gordon, C. P. Hung, and B. J. Lance. EEGNet: A Compact Convolutional Network for EEG-based Brain-Computer Interfaces. *arXiv preprint arXiv:1611.08024*, 2016.
- G. J. McLachlan. *Discriminant Analysis and Statistical Pattern Recognition*. Wiley Series in Probability and Statistics. John Wiley & Sons, Inc., Hoboken, NJ, USA, 3 1992. ISBN 9780471725299. doi: 10.1002/0471725293.
- V. V. Nikulin, G. Nolte, and G. Curio. A novel method for reliable and fast extraction of neuronal EEG/MEG oscillations on the basis of spatio-spectral decomposition. *NeuroImage*, 55(4):1528–1535, 2011.
- F. Pedregosa, G. Varoquaux, A. Gramfort, V. Michel, B. Thirion, O. Grisel, M. Blondel, P. Prettenhofer, R. Weiss, V. Dubourg, et al. Scikit-learn: Machine learning in Python. *Journal of Machine Learning Research*, 12(Oct):2825–2830, 2011.
- R. T. Schirrmeister, J. T. Springenberg, L. D. J. Fiederer, M. Glasstetter, K. Eggenberger, M. Tangermann, F. Hutter, W. Burgard, and T. Ball. Deep learning with convolutional neural networks for EEG decoding and visualization. *Human brain mapping*, 38(11):5391–5420, 2017.
- J. Shamwell, H. Lee, H. Kwon, A. R. Marathe, V. Lawhern, and W. Nothwang. Single-trial EEG RSVP classification using convolutional neural networks. In *Micro-and Nanotechnology Sensors, Systems, and Applications VIII*, volume 9836, page 983622. International Society for Optics and Photonics, 2016.

- S. Taulu and J. Simola. Spatiotemporal signal space separation method for rejecting nearby interference in MEG measurements. *Physics in Medicine & Biology*, 51(7):1759, 2006.
- V. N. Vapnik. *The nature of statistical learning theory*. Springer, 2000. ISBN 9781441931603.
- B. U. Westner, S. S. Dalal, S. Hanslmayr, and T. Staudigl. Across-subjects classification of stimulus modality from human MEG high frequency activity. *PLoS Computational Biology*, 14(3):e1005938, 3 2018. ISSN 15537358. doi: 10.1371/journal.pcbi.1005938.